Research Article

Chao Tan, Ifty Ahmed, Andrew J. Parsons, Chenkai Zhu, Fernando B. Betanzos, Chris D. Rudd, and Xiaoling Liu*

Effects of Fe_2O_3 addition and annealing on the mechanical and dissolution properties of MgO- and CaO-containing phosphate glass fibres for bio-applications

https://doi.org/10.1515/bglass-2018-0006
Received Nov 07, 2017; revised Mar 07, 2018; accepted Apr 21, 2018

Abstract: This paper investigated the preparation of phosphate glass fibres (PGFs) in the following systems: i) $45P_2O_5$-$5B_2O_3$-$5Na_2O$-(29-x)CaO-16MgO-(x)Fe_2O_3 and ii) $45P_2O_5$-$5B_2O_3$-$5Na_2O$-24CaO-(21-x)MgO-(x)Fe_2O_3 (where x = 5, 8 and 11 mol%) for biomedical applications. Continuous fibres of 23 ± 1 μm diameter were prepared via a melt-draw spinning process. Compositions with higher Fe_2O_3 content and higher MgO/CaO ratio required higher melting temperature and longer heating time to achieve glass melts for fibre pulling. The effects of Fe_2O_3 addition and annealing treatment on mechanical properties and degradation behaviours were also investigated. Adding Fe_2O_3 was found to increase the tensile strength from 523 ± 63 (Ca-Fe5) to 680 ± 75 MPa (Ca-Fe11), improve the tensile modulus from 72 ± 4 (Ca-Fe5) to 78 ± 3 GPa (Ca-Fe11) and decrease the degradation rate from 4.0 (Mg-Fe5) to 1.9×10^{-6} kg m^{-2} s^{-1} (Mg-Fe11). The annealing process reduced the fibre tensile strength by 46% (Ca-Fe5), increased the modulus by 19.6% (Ca-Fe8) and decreased the degradation rate by 89.5% (Mg-Fe11) in comparison to the corresponding as-drawn fibres. Additionally, the annealing process also impeded the formation of precipitate shells and revealed co-existence of the precipitation and the pitting corrosion as fibre degradation behaviours.

Keywords: Phosphate glass fibres, iron, mechanical properties, annealing, degradation

1 Introduction

Phosphate glasses can be made with formulations similar to the inorganic component of bone and have been widely investigated as novel biomaterials for bone repair applications [1–4]. They have been produced and processed into different forms such as powders [5], chopped fibres [6, 7] or continuous fibres to reinforce resorbable polymeric matrices [8–11]. It is known that high P_2O_5 content phosphate glasses have low chemical durability due to their susceptibility to hydration and hydrolysis [10]. Conversely, phosphate glasses with higher phosphate content are easier to draw into continuous fibres due to their longer chain structure [12]. In order to improve the fibre drawing performance of more chemically durable and lower content phosphate glasses, B_2O_3 was added to optimise the glass structure as it has been shown that addition of B_2O_3 in-

***Corresponding Author: Xiaoling Liu:** Ningbo Nottingham New Materials Institute, The University of Nottingham Ningbo China, Ningbo, 315100, China; Ningbo Nottingham International Academy for the Marine Economy and Technology, The University of Nottingham Ningbo China, Ningbo, 315100, China; Email: Xiaoling.Liu@nottingham.edu.cn; Tel.: +86 (0)574 8818 2753
Chao Tan: International Doctoral Innovation Centre, The University of Nottingham Ningbo China, Ningbo, 315100, China; Ningbo Nottingham New Materials Institute, The University of Nottingham Ningbo China, Ningbo, 315100, China
Ifty Ahmed, Fernando B. Betanzos: Advanced Materials Research Group, Faculty of Engineering, The University of Nottingham, Nottingham, NG7 2RD, United Kingdom
Andrew J. Parsons: Composites Research Group, Faculty of Engineering, The University of Nottingham, Nottingham, NG7 2RD, United Kingdom
Chenkai Zhu: Ningbo Nottingham New Materials Institute, The University of Nottingham Ningbo China, Ningbo, 315100, China; Ningbo Nottingham International Academy for the Marine Economy and Technology, The University of Nottingham Ningbo China, Ningbo, 315100, China
Chris D. Rudd: Ningbo Nottingham New Materials Institute, The University of Nottingham Ningbo China, Ningbo, 315100, China; Advanced Materials Research Group, Faculty of Engineering, The University of Nottingham, Nottingham, NG7 2RD, United Kingdom; Ningbo Nottingham International Academy for the Marine Economy and Technology, The University of Nottingham Ningbo China, Ningbo, 315100, China

creased the effective phosphate chain lengths (Q^2 species) [13–16] without compromising on chemical durability.

In our previous work [17], phosphate glasses with compositions of $45P_2O_5$-$5B_2O_3$-$5Na_2O$-(29-x)CaO-16MgO-(x)Fe_2O_3 and $45P_2O_5$-$5B_2O_3$-$5Na_2O$-24CaO-(21-x)MgO-(x)Fe_2O_3 (where x = 5, 8 and 11) were prepared and investigated. It was found that the local phosphate network was mainly based on pyro- and metaphosphate units (Q^1 and Q^2) even though the O/P ratio was higher than 3.5. This was due to the addition of B_2O_3, which introduced BO_3/BO_4 units into the phosphate chain structure to form a mixed borophosphate glass. It was anticipated that this extended borophosphate structure would improve fibre drawing performance without suffering the poor chemical durability that would be observed in an extended pure phosphate network.

The degradation rate of resorbable materials plays a very important role for their intended application [18]. In this respect, phosphate glasses offer a distinct advantage over other materials like Si-based bioglass, as their degradation rates can easily be tailored via simply modifying the addition of modifier oxides to suit the end application [7, 13, 19–22]. In addition, it has also been reported that the degradation rate of phosphate glasses has a direct influence on their biological performance, as their biocompatibility is enhanced with higher chemical durability [4, 23–28]. Fe_2O_3 addition to phosphate glasses has successfully been shown to efficiently improve their chemical durability, which in turn showed improvement in the biocompatibility of the glasses [17, 29–33]. However, the study [34] reported that Fe_2O_3 addition could lead to more stringent fibre drawing conditions for phosphate glasses, since the glass drawing temperature was close to the maximum temperature limit for the in-house melt-drawn fibre preparation system that was used.

A number of studies have investigated the effect of iron oxide on phosphate glass systems, such as P_2O_5-Fe_2O_3-BaO [35], P_2O_5-Fe_2O_3-PbO [36] and P_2O_5-Fe_2O_3-TiO_2-CaF_2 [37]. When mono- or divalent metal oxide modifiers were replaced by Fe_2O_3, these studies showed that the phosphate chain structure increased in cross-linking density [17, 38]. Both Fe^{2+} and Fe^{3+} can exist in the iron phosphate glasses, forming strong chemically resistant P-O-Fe(II) and P-O-Fe(III) bonds instead of P-O-P bonds [29, 39]. Furthermore, both Fe^{2+} and Fe^{3+} play different roles in the glass structure, with Fe^{2+} suggested to involved in cross-linking, whereas Fe^{3+} could go in the phosphate network [32]. In the case of P_2O_5-B_2O_3-Na_2O-CaO-MgO-Fe_2O_3, cross-linking between the phosphate chains occurred due to the higher field strength of Fe ions compared to sodium, calcium and magnesium [23, 40, 41], with the ionic radius decreasing for Na^+(1.13 Å) > Ca^{2+}(0.99 Å) > Mg^{2+}(0.72 Å) > Fe^{3+}(0.64 Å) (six-fold coordination for Mg^{2+} and Ca^{2+}) [13, 42]. In addition, Albon *et al.* [29] investigated the P_2O_5-Fe_2O_3-Na_2O glasses by using Mössbauer spectrometry and found an increase in Fe^{3+}/Fe^{2+} ratio with increasing Fe_2O_3 content in the glass. They also observed that the Fe^{2+} ions were oxidized to Fe^{3+} in the glass during the heat treatment. Therefore, it was expected that both Fe_2O_3 content and heat treatment would affect the glass structure and consequently the physical properties.

Phosphate glasses have been prepared into fibres with sufficient mechanical strength for investigations into bone repair applications [1]. Furthermore, phosphate glass fibre (PGF) reinforced polymeric composites have also been manufactured with suitable mechanical strength for use as bone repair devices. For example, the flexural properties of PGF/PLA composites have been reported to be 80-500 MPa for flexural strength and 5-25 GPa for modulus, with varying fibre formulations, fibre volume fractions and fibre alignment [8, 43–45]; while the flexural properties of cortical bone are stated to be 135-193 MPa for strength and 10-20 GPa for modulus [46–48].

The aim of the present work was to utilise the extended borophosphate network structure to improve the fibre drawing characteristics of phosphate glasses containing less than 50% phosphate, whilst investigating the effects of varying the ratio of divalent and trivalent additives (Ca, Mg and Fe) on the mechanical and chemical behaviour. Most studies to date substitute between monovalent and other species, whereas here the exchange is between divalent and trivalent species. The effects of heat treatment on the fibres were also considered. This work will provide glass formulations that provide fibres with superior mechanical and chemical properties, but that are also suited to continuous production as reinforcement materials. The bulk glass of these formulations has been studied previously [17] and the present work analysed the glass fibres from these formulations which has not been investigated before.

2 Materials and methods

2.1 Glass preparation and compositional analysis

Five different glass compositions in two series of $45P_2O_5$-$5B_2O_3$-$5Na_2O$-(29-x)CaO-16MgO-(x)Fe_2O_3 and $45P_2O_5$-$5B_2O_3$-$5Na_2O$-24CaO-(21-x)MgO-(x)Fe_2O_3 (where x = 5, 8 and 11) were prepared via a melt quenching method and

Table 1: The real glass formulations (in mol%) of the batch used for fibre preparation characterized by using ICP-MS, the corresponding O/P ratio and glass transition temperature (T_g) as analysed in previous work [17].

Glass series	Sample codes	P_2O_5	B_2O_3	Na_2O	CaO	MgO	Fe_2O_3	O/P	T_g (°C)
$45P_2O_5$-$5B_2O_3$	Ca-Fe5	44.0 ± 0.1	4.8 ± 0.1	6.2 ± 0.1	23.0 ± 0.1	16.8 ± 0.1	5.3 ± 0.1	3.37	513
-$5Na_2O$-(29-x)CaO	Ca-Fe8	43.6 ± 0.1	4.8 ± 0.1	6.7 ± 0.1	20.3 ± 0.1	16.2 ± 0.1	8.4 ± 0.1	3.45	517
-16MgO-(x)Fe_2O_3	Ca-Fe11	43.4 ± 0.1	4.7 ± 0.1	7.3 ± 0.1	17.4 ± 0.1	16.0 ± 0.1	11.2 ± 0.1	3.52	521
$45P_2O_5$-$5B_2O_3$	Mg-Fe5	44.0 ± 0.1	4.8 ± 0.1	6.2 ± 0.1	23.0 ± 0.1	16.8 ± 0.1	5.3 ± 0.1	3.37	513
-$5Na_2O$-24CaO	Mg-Fe8	43.8 ± 0.1	4.9 ± 0.1	6.8 ± 0.1	23.1 ± 0.1	13.2 ± 0.1	8.2 ± 0.1	3.44	517
-(21-x)MgO-(x)Fe_2O_3	Mg-Fe11	43.7 ± 0.1	4.8 ± 0.1	7.3 ± 0.1	22.7 ± 0.1	10.1 ± 0.1	11.3 ± 0.1	3.51	523

compositionally confirmed by inductively coupled plasma mass spectrometry (ICP-MS) as discussed in the previous work [17]. Table 1 shows the ICP results, O/P ratio and glass transition temperature of the investigated glass batches. In brief, the glass compositions were prepared using reagent grade P_2O_5, B_2O_3, NaH_2PO_4, $CaHPO_4$, $MgHPO_4{\cdot}3H_2O$ and $FePO_4{\cdot}2H_2O$ (Sigma Aldrich, UK) powder precursors which were mixed into a Pt/5% Au crucible (Birmingham Metal Co., UK). After preheating at 350°C for 30 min, the crucible was transferred to a furnace and the salt mixtures were subsequently melted at 1200°C for 90 min. Finally, the molten glass was poured onto a steel plate and left to cool.

2.2 Phosphate glass fibres (PGFs) preparation

Continuous fibres of ~25 µm diameter were produced via a melt-draw spinning process using a dedicated in-house facility [49]. The pulling temperature was adjusted to around 1200°C. The molten glass was pushed through the bushing by hydrostatic pressure and collected on a rotating drum at a speed of 900 rpm.

The resulting fibres were annealed for 90 min at 10°C above the T_g (see Table 1). The heating cycle involved a 5°C min^{-1} ramp to T_g −200°C, followed by 1°C min^{-1} to T_g + 10°C, 90-min dwell and cooling to T_g −200°C by 0.25°C min^{-1} before another 5°C min^{-1} ramp to room temperature.

2.3 Fibre Degradation Analysis

A degradation study was conducted on both the annealed and non-annealed fibres. Around 300 mg fibres, 50 mm length were put into a glass vial containing 30 mL phosphate buffer saline solution (PBS; pH = 7.4 ± 0.1) and the vial was placed into an oven at 37.0 ± 0.5°C. At specified time points, the solution pH was measured. Then the PBS solution was removed carefully and the fibres were dried in a drying oven at 50°C overnight before weighing. The mass loss per surface area of the fibres was plotted against the immersion time to explore the degradation rate ($kg\ m^{-2}\ s^{-1}$). This analysis was carried out for 28 days (time points of 0, 1, 7, 14, 21 and 28) and the PBS solution was changed at each time point.

2.4 Single fibre tensile test (SFTT)

SFTT was conducted in accordance with ISO 11566 [49]. Thirty fibres were mounted individually onto plastic tabs for each sample with a 25-mm-gauge length testing setup. The ends of each fibre were bonded to the plastic tab with an acrylic adhesive (Dymax 3099, Dymax, Europe) and the adhesive was cured using UV light. The diameter of the fibres was measured using an LSM 6200 laser scan micrometre (Mitutoyo, Japan), which was previously calibrated with the glass fibre of known diameter (determined by SEM) and the error on diameter measurements was considered to be ±0.3 µm [34]. The tensile test was performed using a LEX 810 tensile tester (Diastron, UK) at room temperature with a load cell capacity of 1 N and a crosshead speed of 0.017 mm s^{-1}.

The Weibull distribution is an accepted statistical tool used to characterise the failure mode of brittle fibres [50]. The Weibull modulus and normalising stress are described as the shape and scale parameters, respectively, where the normalising stress (Weibull scale) can be regarded as the most probable stress at which a fibre of gauge length will fail [34]. In this study, Weibull parameters were obtained from the tensile strength data calculated using Minitab 15 (version 3.2.1).

2.5 Scanning electron microscopy (SEM) analysis

SEM images were taken to examine the change in surface morphology of the annealed and non-annealed fibres. The chopped fibres were fixed on a sample stage with conductive adhesive tape and coated with gold using a Leica EM SCD 500 high vacuum sputter coater prior to use. The micrographs were taken at an accelerating voltage of 3 kV using SE2 mode on a Zeiss Sigma/VP SEM.

2.6 Statistical analysis

The statistical analysis was performed using the IBM SPSS (version 22). A Student's unpaired t-test was used to analyse the significance of the difference between different samples, assuming equal variance and determining two-tailed p-values. One-way analysis of variance (ANOVA) was calculated with the Bonferroni post-test to compare the significance of the change in the factors with iron content or time. The threshold value chosen for statistical significance was at the 0.05 level.

3 Results

3.1 Mechanical properties of as-drawn fibres

As shown in Figure 1a, a significant increase ($p < 0.05$) in tensile strength of the fibres was observed with increasing Fe_2O_3 content at the expense of CaO/MgO. The values obtained were 523 ± 63, 587 ± 72 and 680 ± 75 MPa for Ca-Fe5, 8 and 11 fibres, respectively; whilst 523 ± 63, 561 ± 75 and 605 ± 72 MPa were obtained for Mg-Fe5, 8 and 11 fibres, respectively. No significant difference in tensile strength was observed between the glass series with the substitution of CaO and MgO. Table 2 represents the Weibull distribution of fibre strength. It was noted that the trend of normalising strength was consistent with that of mean tensile strength. The Weibull modulus of the fibres was seen to range from 6.0 to 8.7. Figure 2 shows an example of the Weibull plots.

Figure 1b shows a significant increase ($p < 0.001$) in tensile modulus and the values were 72 ± 4, 74 ± 2 and 78 ± 3 GPa for Ca-Fe5, 8 and 11 fibres, respectively. These values of modulus were numerically same as that of the Mg-Fe5, 8 and 11 fibres, respectively.

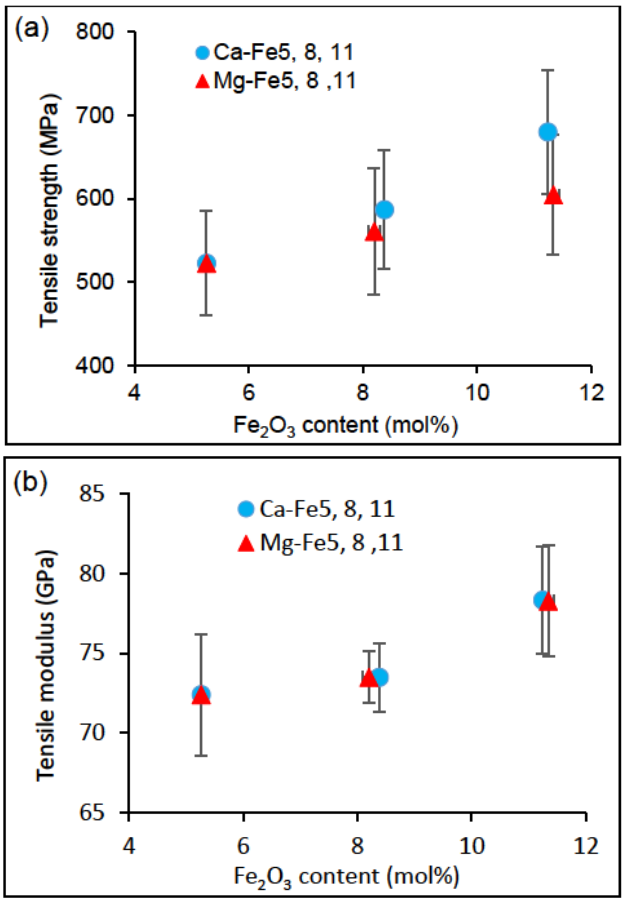

Figure 1: Tensile (a) strength and (b) modulus of as-drawn fibres of the composition Ca-Fe5, 8, 11 and Mg-Fe5, 8, 11 against Fe_2O_3 content ($n = 30$).

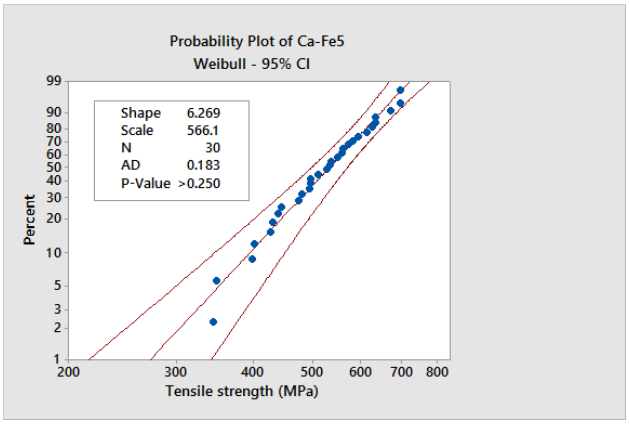

Figure 2: Weibull analysis of Ca-Fe5 was completed from the tensile strength data calculated using Minitab.

3.2 Mechanical properties of annealed fibres

The effect of annealing on mechanical properties was analysed. Figure 3a and b showed a decrease in tensile strength

Table 2: Weibull distribution of as-drawn fibres of the composition Ca-Fe5, 8, 11 and Mg-Fe5, 8, 11 (n = 30). The tensile strength values are also included for ease of comparison.

Sample codes	Diameter (µm)	Tensile strength (MPa)	Normalising strength (MPa)	Weibull modulus
Ca-Fe5	24.2 ± 1.2	523 ± 63	566	6.3
Ca-Fe8	22.2 ± 3.1	587 ± 72	663	6.3
Ca-Fe11	23.2 ± 1.9	680 ± 75	764	6.0
Mg-Fe5	24.2 ± 1.2	523 ± 63	566	6.3
Mg-Fe8	21.5 ± 1.9	561 ± 75	613	8.7
Mg-Fe11	23.4 ± 0.9	605 ± 72	682	6.5

and an increase in tensile modulus for the annealed fibres, respectively. The strength values of non-annealed fibres were shown in Table 2 and the values of annealed fibres were observed to be 280 ± 81 MPa for Ca-Fe5, 374 ± 65 MPa for Ca-Fe8, 485 ± 55 MPa for Ca-Fe11, 280 ± 81 MPa for Mg-Fe5, 330 ± 55 MPa for Mg-Fe8 and 408 ± 78 MPa for Mg-Fe11. Thus, the reductions in tensile strength after the annealing process were found to be by 46%, 36% and 29% of the as-drawn Ca-Fe5, 8 and 11 fibres ($p < 0.001$), respectively; while the reductions were found to be by 46%, 41% and 32% of the as-drawn Mg-Fe5, 8 and 11 fibres ($p < 0.001$), respectively.

According to Figure 3b, the tensile modulus of the annealed fibres were observed to be 84 ± 3 GPa for Ca-Fe5, 88 ± 4 GPa for Ca-Fe8, 91 ± 2 GPa for Ca-Fe11, 84 ± 3 GPa for Mg-Fe5, 87 ± 2 GPa for Mg-Fe8 and 91 ± 5 GPa for Mg-Fe11. Thus, the tensile modulus of the annealed fibres were observed to increase by 16.5% for Ca-Fe5, 19.6% for Ca-Fe8, 16.3% for Ca-Fe11, 16.5% for Mg-Fe5, 18.0% for Mg-Fe8 and 15.6% for Mg-Fe11 ($p < 0.001$) compared to the corresponding as-drawn fibres.

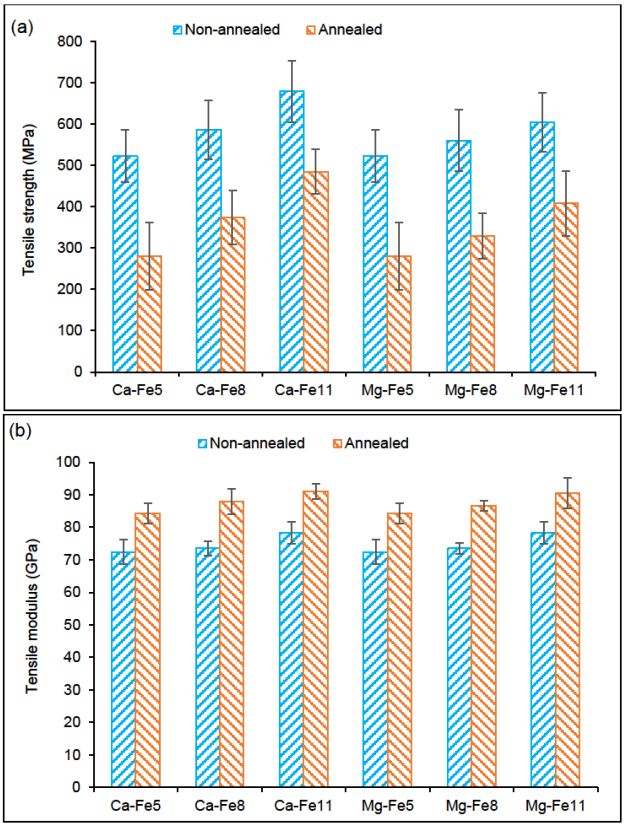

Figure 3: Tensile (a) strength and (b) modulus of non-annealed and annealed fibres of the composition Ca-Fe5, 8, 11 and Mg-Fe5, 8, 11 (n = 30).

3.3 Mechanical properties of degraded non-annealed fibres

Figure 4a shows the tensile strength of non-annealed glass fibres versus degradation time. It was observed that the tensile strength decreased rapidly during the earlier time points and then increased for day 14. After 1 day immersion, the tensile strength for Ca-Fe5, 8 and 11 fibres decreased from 523 ± 63, 587 ± 72 and 680 ± 75 MPa to 456 ± 61, 345 ± 81 and 485 ± 98 MPa, respectively. With further immersion up to 7 days, the strength of Ca-Fe5, 8 and 11 fibres decreased to 323 ± 48, 257 ± 52 and 300 ± 84 MPa, respectively. Thus, at day 7 the reduction in strength observed was 38%, 56% and 56% of the as-drawn Ca-Fe5, 8 and 11 fibres, respectively. However, an increase in tensile strength was observed for the 14 days-degraded fibres compared to the 7 days-degraded fibres, and the values of tensile strength at day 14 were 449 ± 54, 318 ± 91 and 439 ± 86 MPa for Ca-Fe5, 8 and 11 fibres, respectively. Furthermore, no statistically significant difference in tensile strength was observed between the 0, 1, 7 and 14 days-degraded fibres.

The variance in tensile strength of Mg-Fe5, 8 and 11 fibres shows a similar trend with that of Ca-Fe5, 8 and 11

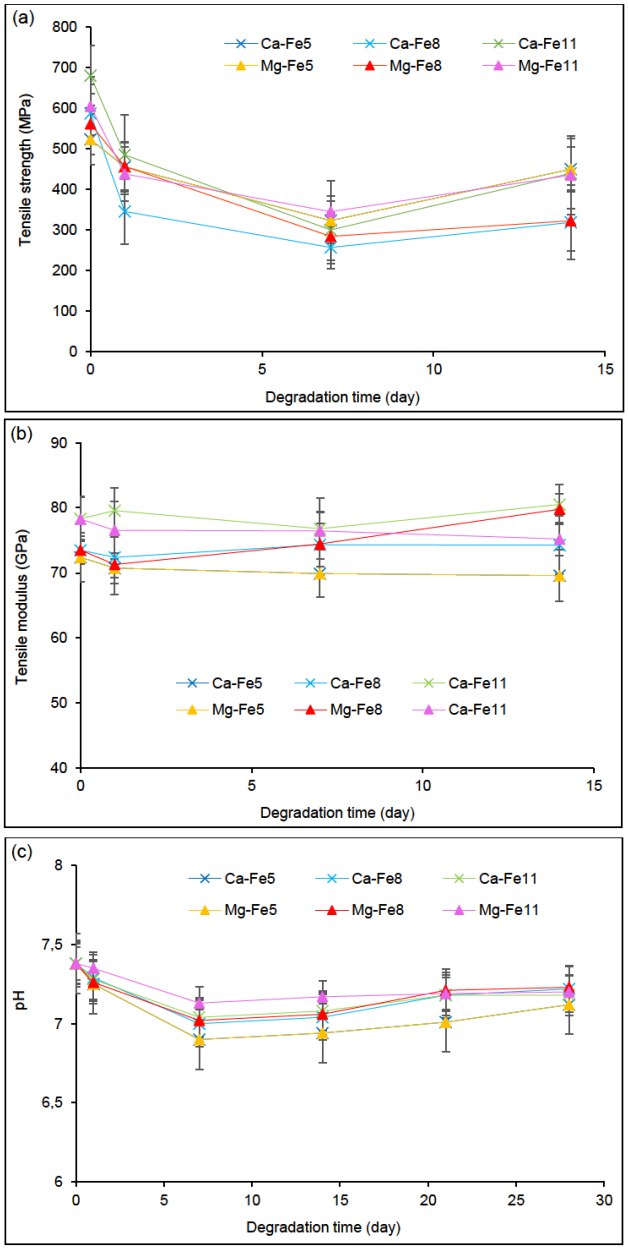

Figure 4: Tensile (a) strength and (b) modulus of non-annealed fibres of the composition Ca-Fe5, 8, 11 and Mg-Fe5, 8, 11 during degradation in PBS solution at 37°C and the pH (c) of the corresponding solutions ($n \geq 20$). The lines are drawn as a guide for the eye.

fibres. After 1 day immersion, the tensile strength for Mg-Fe5, 8 and 11 fibres decreased from 523 ± 63, 561 ± 75 and 605 ± 72 MPa to 456 ± 61, 456 ± 57 and 438 ± 67 MPa, respectively. At day 7 the strength became 323 ± 48, 284 ± 59 and 345 ± 77 MPa for Mg-Fe5, 8 and 11 fibres, respectively, which shows a reduction by 38%, 49% and 43% of the as-drawn Mg-Fe5, 8 and 11 fibres, respectively. Moreover, at day 14 the tensile strength of Mg-Fe5, 8 and 11 fibres was observed to be 449 ± 54, 323 ± 75 and 435 ± 97 MPa, respectively. Also, no statistically significant difference in tensile strength was observed between the 0, 1, 7 and 14 days-degraded fibres.

Figure 4b shows the tensile modulus of the corresponding degraded fibres. No statistically significant difference in fibre tensile modulus was observed throughout the degradation period.

Figure 4c shows the pH of the corresponding solutions, which endured at 7.18 ± 0.14 for the whole degradation period, even though there was a slight decrease in pH during the early immersion period.

The micrographs in Figure 5 exhibit the corresponding surface morphologies of the degraded fibres. The morphologic changes in fibres revealed the effects of different immersion time and glass compositions. The cracked outer shells were observed with the degrading glass fibres.

3.4 Mechanical properties of degraded annealed fibres

Figure 6a shows the tensile strength of annealed glass fibres versus degradation time. Similar to the non-annealed fibres, a decrease in tensile strength was observed from day 1 to day 7, while an increase was seen from day 7 to day 14. However, no evident trend was found for the change of tensile strength on day 1 immersed samples. From day 1 to day 7, the tensile strength for Ca-Fe5, 8 and 11 fibres decreased from 325 ± 72, 385 ± 76 and 358 ± 63 MPa to 220 ± 49, 259 ± 77 and 283 ± 64 MPa, respectively, which shows a reduction by 21%, 31% and 42% of the corresponding day-0 fibres, respectively. At day 14, the tensile strength became 293 ± 62, 289 ± 71 and 319 ± 65 MPa for Ca-Fe5, 8 and 11 fibres, respectively. No statistically significant change ($p > 0.05$) in tensile strength was observed between the 0, 1, 7 and 14 days-degraded fibres.

Moreover, at day 1, the tensile strength of Mg-Fe5, 8 and 11 fibres were observed to be 325 ± 72, 354 ± 73 and 323 ± 86 MPa, respectively. At day 7, the values of tensile strength became 220 ± 49, 280 ± 67 and 260 ± 69 MPa for Mg-Fe5, 8 and 11 fibres, respectively, which shows a reduction by 21%, 15% and 36% of the corresponding day-0 fibres, respectively. At day 14, the strength values were observed to be 293 ± 62, 317 ± 63 and 307 ± 64 MPa for Mg-Fe5, 8 and 11 fibres, respectively. Also, no statistically significant change ($p > 0.05$) in tensile strength was observed between the 0, 1, 7 and 14 days-degraded fibres.

Figure 6b shows the tensile modulus of the corresponding degraded fibres. No statistically significant

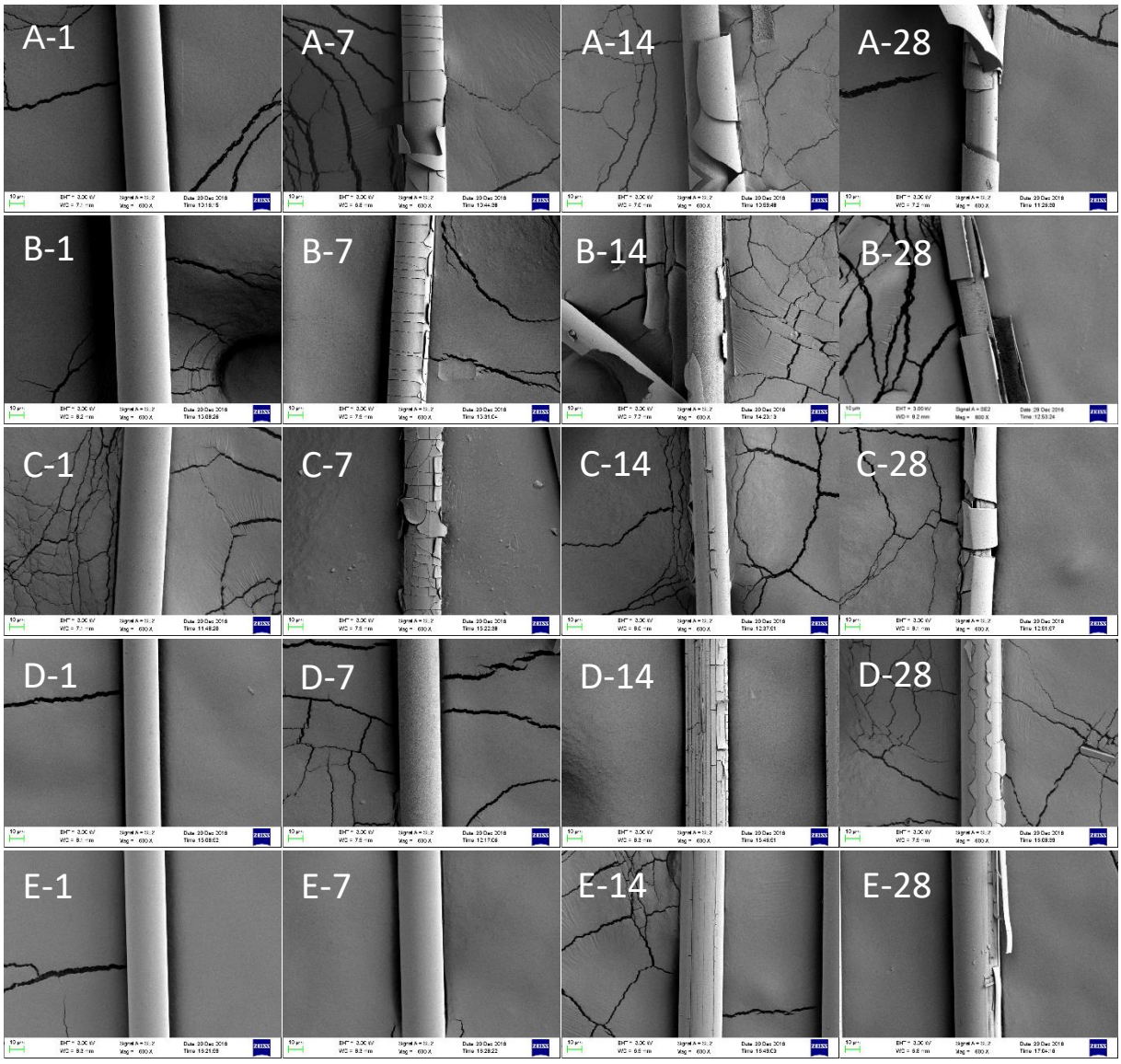

Figure 5: Scanning electron microscopy of day 1, 7, 14 and 28 non-annealed degraded fibres of the composition Ca-Fe5/Mg-Fe5 (A1-A28), Ca-Fe8 (B1-B28), Mg-Fe8 (C1-C28), Ca-Fe11 (D1-D28) and Mg-Fe11 (E1-E28). The cracked base shows the conductive tape.

change ($p > 0.05$) in the fibre tensile modulus was observed throughout the degradation study.

Figure 6c shows the pH of the corresponding solutions, which remained at 7.36 ± 0.04 throughout the degradation study.

It was also observed from Figure 7 that the annealed fibres underwent a surface pitting during degradation, which was seen to be distributed heterogeneously along the fibre surface.

3.5 Degradation rates of fibres

Figure 8 represents degradation rates of the non-annealed and annealed fibres after 28-days degradation in PBS solution at 37°C. A 20-36% reduction in degradation rate of non-annealed fibres was observed for each 3 mol% Fe_2O_3 increment at the cost of CaO/MgO. After 28 days, the degradation rates were observed to be 39.6, 30.7 and 24.5 × 10^{-7} kg m^{-2} s^{-1} for the non-annealed Ca-Fe5, 8 and 11 fibres, respectively, while the values were 39.6, 29.4 and 18.7 × 10^{-7} kg m^{-2} s^{-1} for the non-annealed Mg-Fe5, 8 and 11 fibres, respectively. No significant difference in degradation

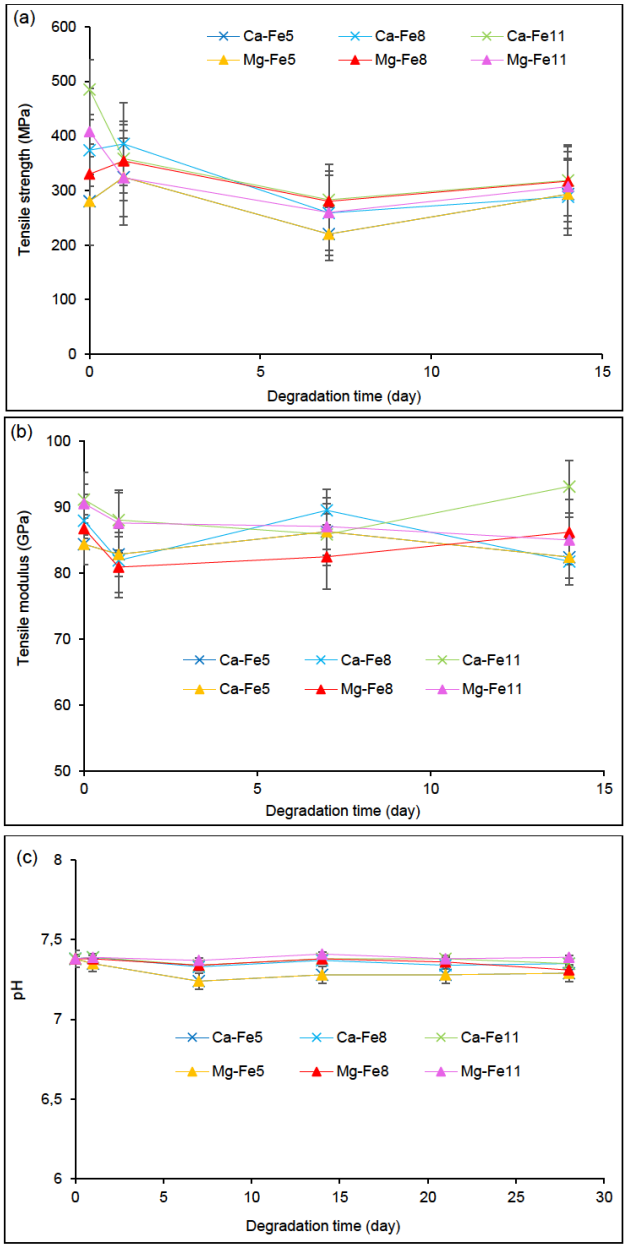

Figure 6: Tensile (a) strength and (b) modulus of annealed fibres of the composition Ca-Fe5, 8, 11 and Mg-Fe5, 8, 11 during degradation in PBS solution at 37°C and the pH (c) of the corresponding solutions ($n \geq 20$). The lines are drawn as a guide for the eye.

rate was found between the glass compositions with the replacements of CaO and MgO.

Similar trends were found for the annealed fibres and the degradation rate decreased by 38%-73% for each 3 mol% Fe_2O_3 increment instead of CaO/MgO. The degradation rates were observed to be 11.7, 6.3 and 3.2×10^{-7} kg m^{-2} s^{-1} for the annealed Ca-Fe5, 8 and 11 fibres, respectively, and to be 11.7, 7.3 and 2.0×10^{-7} kg m^{-2} s^{-1} for the annealed Mg-Fe5, 8 and 11 fibres, respectively. Thus, the annealing was observed to reduce the degradation rate by 70.4%, 79.9% and 86.9% for the Ca-Fe5, 8 and 11 fibres, respectively; while the degradation rate decreased by 70.4%, 75.3% and 89.5% for the Mg-Fe5, 8 and 11 fibres, respectively.

The decrease in degradation rate of non-annealed and annealed fibres with increasing Fe_2O_3 content at the cost of CaO/MgO was shown to be statistically significant ($p < 0.05$) via ANOVA data.

4 Discussion

In this study, continuous fibre was achieved for all the formulations investigated, with no breakage for at least 3 hours. As expected, the empirical evidence showed that the compositions with higher Fe_2O_3 content and higher MgO/CaO ratio required higher melting temperatures and longer heating times to achieve suitable glass melts for fibre pulling.

4.1 Mechanical properties of as-drawn fibres

Generally, the mechanical properties of the fibres are strongly dependent on the glass formulation [34, 51]. Higher phosphate content in phosphate glasses normally results in longer phosphate chain length in the glass network [52]. The longer chain contributes to the higher mechanical strength of the fibres [53–55]. The higher field strength of the modifier ions can also increase the fibre strength by strengthening the cross-linking between phosphate chains [9, 56]. In this case, the addition of Fe_2O_3 leads to the stronger P-O-Fe bonds instead of P-O-P in the chain, enhancing the mechanical properties and chemical durability, although the replacement of CaO/MgO by Fe_2O_3 might increase the ionic bonds in the glass network [32, 57, 58]. Ma *et al.* [59] also stated that the dissolution behaviour of P_2O_5-Na_2O-Fe_2O_3 glasses was much more dependent on iron content than the O/P ratio. Moreover, the higher field strength of iron ions than that of calcium and magnesium ions resulted in the stronger cross-linking within the glass structure, which could also be responsible for the increase in tensile strength and modulus of the fibres (see Figure 1a and 1b). Kurkjian [60] studied the mechanical properties of fibres drawn from a metaphosphate glass composition P_2O_5-Al_2O_3-MgO-K_2O and a pyrophosphate glass composition P_2O_5-Fe_2O_3. They suggested that replacing monovalent cations with

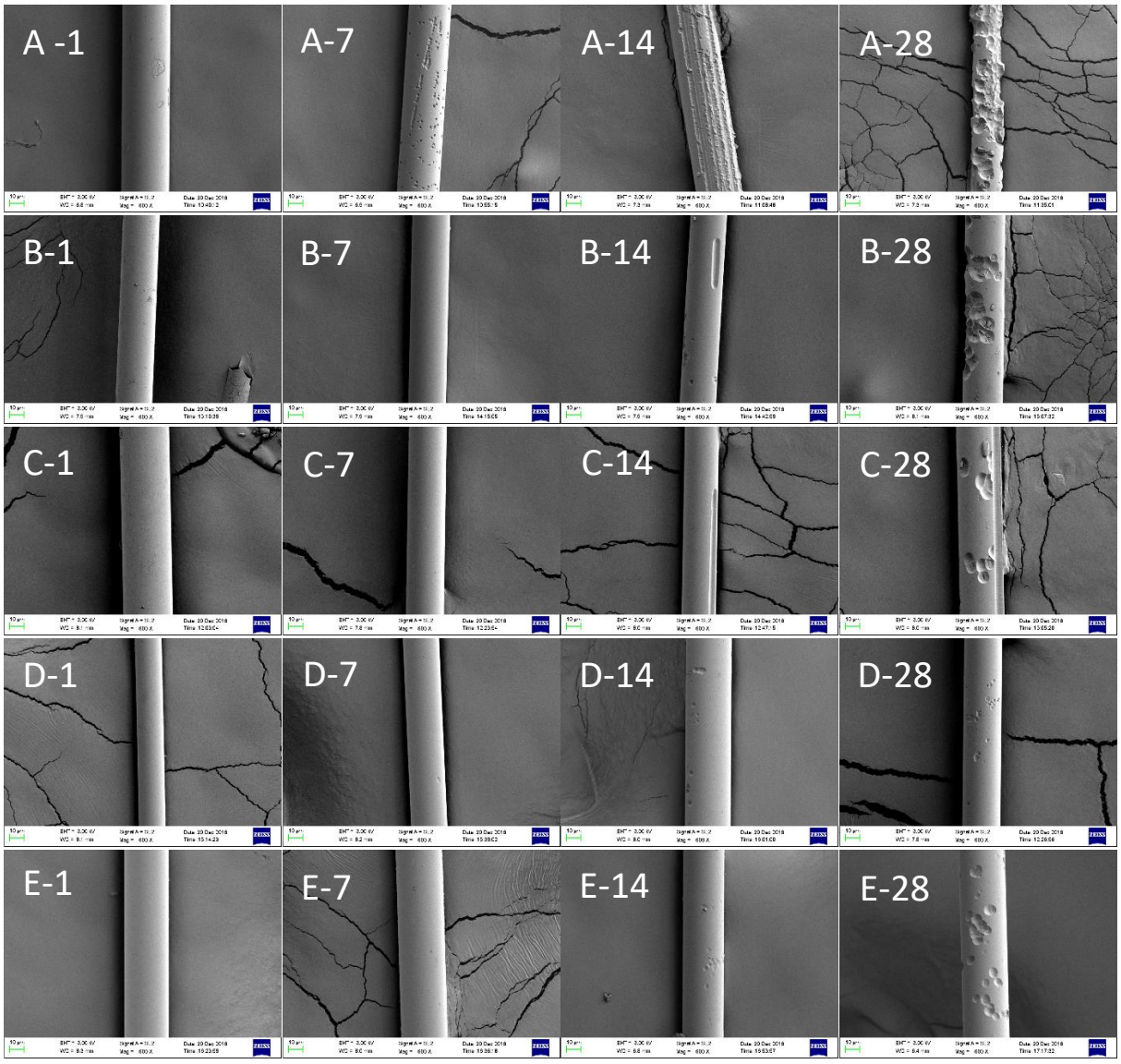

Figure 7: Scanning electron microscopy of day 1, 7, 14 and 28 annealed degraded fibres of the composition Ca-Fe5/Mg-Fe5 (A1-A28), Ca-Fe8 (B1-B28), Mg-Fe8 (C1-C28), Ca-Fe11 (D1-D28) and Mg-Fe11 (E1-E28). The cracked base shows the conductive tape.

trivalent/divalent iron increased the strength and modulus of the PGFs, which was suggested to be due to the higher cross-linking density between the phosphate chains caused by the higher Fe-O bond strength [23, 40].

Lin *et al.* [61] produced P_2O_5-CaO-Fe_2O_3 glass fibres with diameter of ~20 µm and investigated the effect of Fe_2O_3 addition on the properties of the fibres. The tensile strength of the fibres was observed to increase from ~600 to ~1000 MPa and the modulus increased from ~43 to ~64 GPa, as Fe_2O_3 content increased from 5 to 22 wt%. This increase in mechanical properties was attributed to the formation of cross-linked Fe-O-P chains. Murgatroyd [62] stated that for the purpose of fibre drawing, a number of strong bonds are required to withstand the stresses from the pulling process at high temperature. The continuity of a fibre drawing process depends on the ability of the strongest bonds to hold together as they are pulled out of the melt. In PGFs, the strongest bonds normally present the P-O bonds in the phosphate chain [63, 64]. The addition of Fe_2O_3 led to a replacement of P-O-P by stronger P-O-Fe bonding [57], which increased bonding strength of the phosphate chains, resulting in an improvement in tensile strength of the fibres.

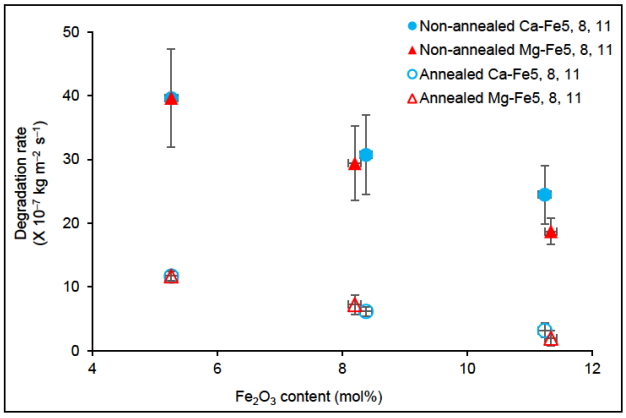

Figure 8: Degradation rates of non-annealed and annealed fibres of the composition Ca-Fe5, 8, 11 and Mg-Fe5, 8, 11 against Fe_2O_3 content (n = 3).

4.2 Dissolution properties of non-annealed fibres

As shown in Figure 4a, the tensile strength of the fibres was observed to decrease rapidly during the earlier immersing period and then increase for day 14. A similar observation was reported in the case of P_2O_5-B_2O_3-CaO-MgO-Na_2O glass fibres [9], where the results presented a rapid loss of strength after 1 day immersion and a cumulative reduction by almost half of the initial values at day 7. However, an increase in tensile strength was observed from day 7 to day 14. This has been previously explained as the penetration of water molecules and Na^+-H^+ exchange. The contact with aqueous media will lead to the Na^+-H^+ exchange to form a hydrated layer and the diffusion of water will be impeded by the increasing thickness of the hydrated layer.

It is widely accepted that the dissolution mechanism of phosphate glasses mainly consists of two processes: dissolution by hydration of entire chains and hydrolysis of P-O-P bonds as initially proposed by Bunker *et al.* [65, 66]. Once immersed in aqueous solution, the hydrated phosphate chains are released into solution, where there undergo hydrolysis. However, an initial pH decrease (from 7.4 ± 0.1 in day-0 to 7.0 ± 0.1 in day-7) was observed in this case (see Figure 4), which was suggested to be a result of phosphate anions in solution released into the media, potentially creating acidic species [67–69]. The dissolved phosphate chains broke down to orthophosphate ultimately via hydrolysis in solution [66], leading to saturation of the media and precipitate formation in static environment. As shown in Figure 9a, the granulate layers were found at the fibre surface and the inner wall of the shell, which were most likely to be the uniformly distributed phosphate precipitates, indicating that the precipitates formed layer by layer during degradation. Such a layer was also found by Clément *et al.* [70] when they investigated the dissolution properties of P_2O_5-CaO-Na_2O glasses in SBF. The Raman results indicated depolymerisation of the phosphate chains due to the hydration reaction at the surface of the glass slabs. An interaction was observed between the hydrated layer at the surface of the glass and the surrounding media, resulting in a thin layer covering the glass sample. The Raman and EDX analysis indicated that this layer was composed of calcium orthophosphate groups. Abou Neel *et al.* [71] also suggested the precipitation of Ca-P at the surface of the P_2O_5-CaO-Na_2O-Fe_2O_3 glass fibres via ion release studies. However, it should be noted that their investigation was conducted in deionised water, which means that the cation of the precipitation came from the glass itself.

It was observed from Figure 9b that the outer shell remained at day 28, whilst the fibre core had undergone further degradation. The precipitated layer seems to be much more durable than the original glass and shows the potential to protect the inner glass from further degradation. However, this layer became very brittle after drying and disintegrated from the surface during sample preparation.

As expected, no significant change in fibre modulus was found during degradation since there was no change in the intrinsic glass structure caused by the degradation as it surface eroded [72].

Figure 8 shows that adding Fe_2O_3 instead of CaO/MgO caused an approximate linear decrease in degradation rate. This increase in glass durability was also correlated with the micrographs shown in Figure 5. A number of studies [32, 57, 58] have given evidence for the enhancement of chemical durability of phosphate glasses caused by Fe_2O_3 addition and suggested that it was attributed to the replacement of P-O-P bonds by more hydration resistant P-O-Fe bonds and the stronger cross-linking between phosphate chains. Yu *et al.* [32] investigated the chemical durability of the P_2O_5-Na_2O-Fe_2O_3 glass with varying Fe_2O_3 content and determined the amount of Fe^{2+} and Fe^{3+} ions via Mössbauer spectroscopy. They found both the Fe^{2+} and Fe^{3+} ions in the phosphate glasses and the concentration of Fe^{3+} increased with increasing Fe_2O_3 content. They concluded that Fe in the form Fe^{3+} strengthened the structure of the glasses like a network former. Thus, they supposed that the Fe^{3+}/Fe^{2+} ratio should be as high as possible for maximum chemical durability of the iron-containing phosphate glass. This supposition was also agreed by Mesko *et al.* [73].

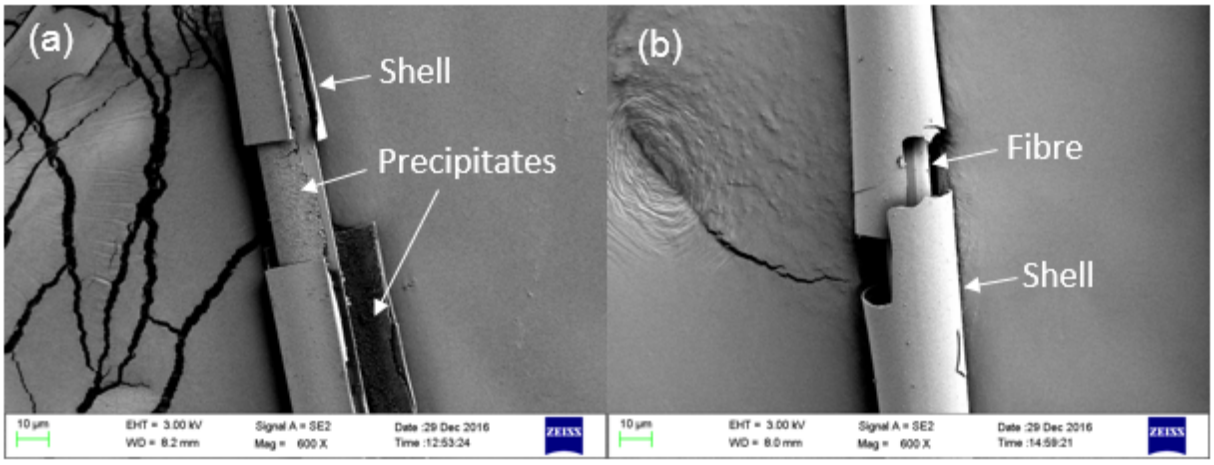

Figure 9: Micrographs for the 28 days-degraded non-annealed (a) Mg-Fe8 and (b) Ca-Fe8 fibres. The cracked base shows the conductive tape.

4.3 Mechanical and dissolution properties of annealed fibres

The fibre pulling process has been shown to orientate the phosphate units along the fibre axis [62, 74, 75]. The rapid cooling will freeze the phosphate chains and the ionic bonds, which makes a highly reactive glass with inherent stresses [76]. The heat-treatment (annealing) process can allow the orientated chains to relax, removing this anisotropy in the fibres and reducing the residual stresses [74, 77, 78].

According to Figure 3a and 3b, the annealing shows a decrease in tensile strength ($p < 0.001$) and an increase in tensile modulus ($p < 0.05$) of the fibres. Similar observations were reported previously in the case of P_2O_5-CaO-MgO-Na_2O [72] and P_2O_5-B_2O_3-CaO-MgO-Na_2O glass fibres [9]. The increase in Young's modulus was suggested to be due to the more stable and compact glass structure. On the other hand, the enhancements of stability and cross-linking density decreased the dissolution rate of the fibres (see Figure 8) by reducing the chemical reactivity of the glass and impeding the water diffusion through the glass network, respectively.

Choueka *et al.* [76] stated that annealing of fibres close to the T_g could stabilize the bonds in the glass; however, the strength might be decreased as the properties of the fibre approached those of bulk glass. Furthermore, the loss of tensile strength could be explained with multiple factors such as manual handling. The pulling and quenching process will generate compressive stresses within the fibre. However, re-heating can cause a relaxation of compressive stresses and even a shrinkage of the fibre which may generate a tensile stress [79]. The high temperature during annealing can also accelerate the interaction between the fibre surface and the moisture in the air [66] and the rapid loss of properties of PGFs can be ascribed to water attacking weak spots in the fibre surface that are under stress [80]. As shown in Figure 10b, the pits next to the white line were observed to arrange in line, while the rest of the pits were seen to be distributed randomly. The regularly distributed pits might indicate that pitting could be initiated from the fibre surface defect [77, 78]. Another example is shown in Figure 10c as the groove on the fibre which might occur due to a scratch on the fibre surface. The annealing operation may increase opportunities of surface damage, which may behave as stress concentration sites [81].

According to the morphological examinations, the annealed fibres in the same composition as that of non-annealed fibres exhibited heterogeneous depressions during degradation (see Figure 7). This type of pitting corrosion in the surface of annealed fibres was also observed by Choueka *et al.* [76] and Cozien-Cazuc *et al.* [20]. With a comparison between Figure 5 and Figure 7, it was noticed that non-annealed and annealed fibres underwent quite different degradation behaviours, which was suggested to be due to the rearrangement of the glass structure during annealing. The ion leach and exchange in dissolution process is believed to occur on sites of structural flaws where concentration of terminal cations interrupts the phosphate network [78]. The structural anisotropy occurs during the fibre drawing process and the terminal cations present a relative regular distribution [82]. Therefore, the diffusion-controlled leaching distributes uniformly at the surface of the fibre. However, annealing can relax the phosphate chains and disrupt them into a disordered en-

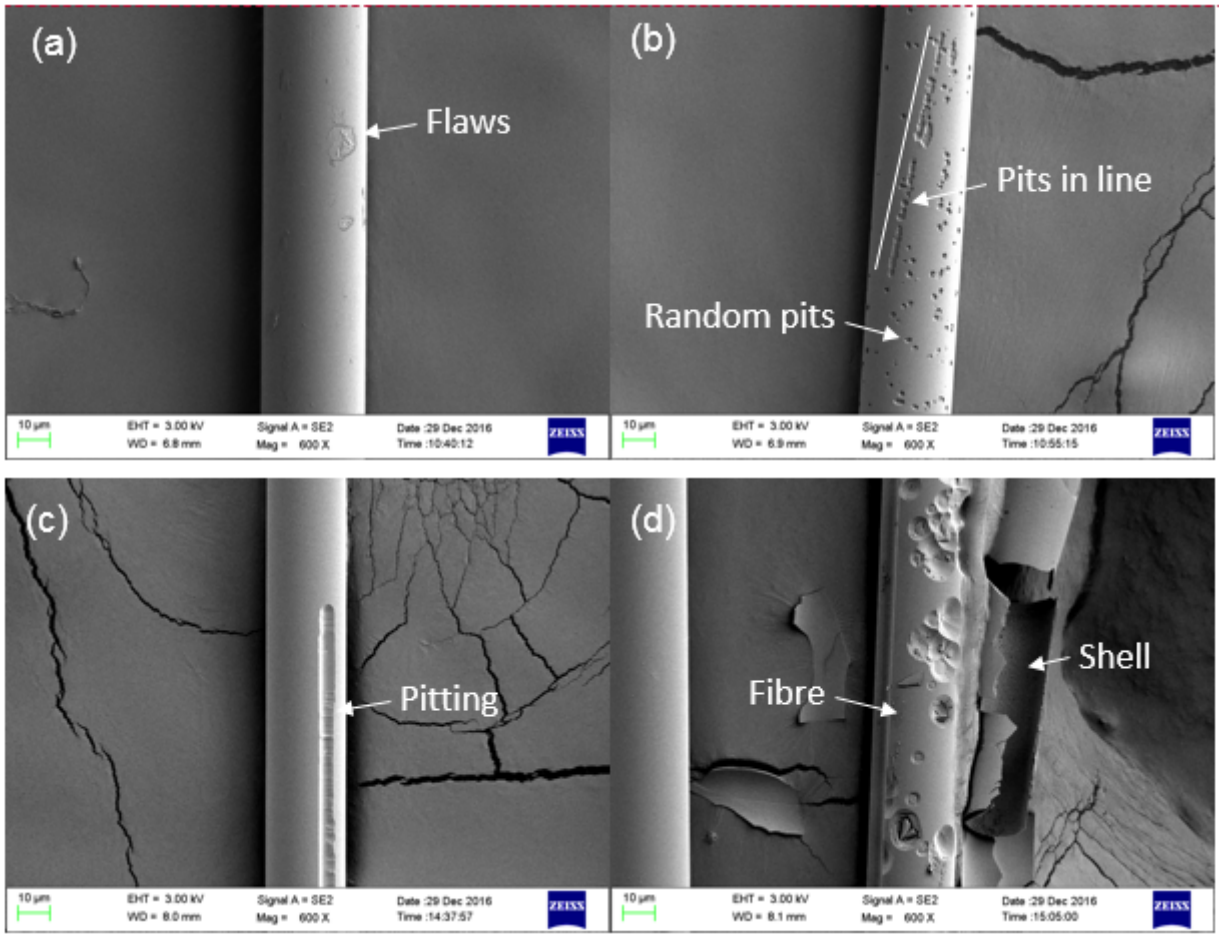

Figure 10: Micrographs for (a) 1 day-degraded annealed Ca-Fe5 fibre, (b) 7 days-degraded annealed Ca-Fe5 fibre (the white line is drawn as a guide for the line-arranged pits), (c) 14 days-degraded annealed Ca-Fe8 fibre and (d) 28 days-degraded annealed Ca-Fe8 fibre. The cracked base shows the conductive tape.

tangled structure, leading to an irregular distribution of structural flaws and resulting in a non-uniform water corrosion [72, 74]. In addition, the precipitate shells and the etch pits could coexist (see Figure 10d), which was also reported by Clément *et al.* [70].

In summary, an approximate linear increase in mechanical properties (tensile strength and modulus) and chemical durability were found with increasing Fe_2O_3 content at the expense of CaO/MgO, which was suggested to be due to the formation of P-O-Fe bonds instead of P-O-P and the stronger cross-linking between phosphate chains. The annealing process was observed to increase the tensile modulus and chemical durability due to the loss of structural anisotropy and the relaxation of residual stresses in the glass fibres. Moreover, a reduction in tensile strength was suggested to be attributed to the relaxation of the compressive stresses, the interaction between the glass and moisture and the surface damage during annealing operation. These behaviours showed a good agreement with the morphologic examination, which described the formation of precipitate shells and pitting corrosion during degradation.

5 Conclusions

The inclusion of B_2O_3 made the fibre preparation continuous with no breakage for at least 3 hours for all five glass formulations. The composition with a higher Fe_2O_3 content and MgO/CaO ratio was observed to require higher melting temperature and longer heating time to achieve suitable glass melts for fibre pulling. The addition of Fe_2O_3 content revealed an increase in tensile strength of the fibres, whilst the annealing process decreased the strength. Chemical durability of the fibres was improved by both Fe_2O_3 addition and the annealing treatment. The annealing process also impeded the precipitation reaction at the

fibre surface and revealed that pitting corrosion dominated the degradation behaviour of some PGFs.

Acknowledgement: The authors kindly acknowledge the financial support from Ningbo Education Bureau, Ningbo Science and Technology Bureau, China's MOST and The University of Nottingham. Additionally, author also would like to appreciate the financial supported by Ningbo S&T bureau Ningbo International Collaboration Project (project code 2017D10012), and Ningbo 3315 Innovation team Scheme "Composites Development and Manufacturing for Sustainable Environment".

Conflict of interest: The authors state no conflict of interest.

Ethical approval: The conducted research is not related to either human or animals use.

References

[1] A. J. Parsons, I. Ahmed, P. Haque, B. Fitzpatrick, M. I. K. Niazi, G. S. Walker, et al., Phosphate glass fibre composites for bone repair, J Bionic Eng, vol. 6, pp. 318-323, 2009.

[2] I. Ahmed, M. Lewis, I. Olsen, and J. C. Knowles, Phosphate glasses for tissue engineering: Part 1. Processing and characterisation of a ternary-based P2O5–CaO–Na2O glass system, Biomaterials, vol. 25, pp. 491-499, 2004.

[3] E. A. Abou Neel, W. Chrzanowski, and J. C. Knowles, Effect of increasing titanium dioxide content on bulk and surface properties of phosphate-based glasses, Acta Biomater, vol. 4, pp. 523-34, May 2008.

[4] E. A. Abou Neel and J. C. Knowles, Physical and biocompatibility studies of novel titanium dioxide doped phosphate-based glasses for bone tissue engineering applications, J Mater Sci Mater Med, vol. 19, pp. 377-86, Jan 2008.

[5] D. S. Brauer, C. Russel, S. Vogt, J. Weisser, and M. Schnabelrauch, Fabrication and in vitro characterization of porous biodegradable composites based on phosphate glasses and oligolactide-containing polymer networks, J Biomed Mater Res A, vol. 80, pp. 410-20, Feb 2007.

[6] Z. Mohammadi, A. S. Mesgar, and F. Rasouli-Disfani, Reinforcement of freeze-dried chitosan scaffolds with multiphasic calcium phosphate short fibers, J Mech Behav Biomed Mater, vol. 61, pp. 590-9, Aug 2016.

[7] R. M. Felfel, I. Ahmed, A. J. Parsons, G. Palmer, V. Sottile, and C. D. Rudd, Cytocompatibility, degradation, mechanical property retention and ion release profiles for phosphate glass fibre reinforced composite rods, Mater Sci Eng C Mater Biol Appl, vol. 33, pp. 1914-24, May 1 2013.

[8] I. Ahmed, I. A. Jones, A. J. Parsons, J. Bernard, J. Farmer, C. A. Scotchford, et al., Composites for bone repair: phosphate glass fibre reinforced PLA with varying fibre architecture, J Mater Sci-Mater M, vol. 22, pp. 1825-1834, 2011.

[9] N. Sharmin, A. J. Parsons, C. D. Rudd, and I. Ahmed, Effect of boron oxide addition on fibre drawing, mechanical properties and dissolution behaviour of phosphate-based glass fibres with fixed 40, 45 and 50 mol% P2O5, J Biomater Appl, vol. 29, pp. 639-53, Nov 2014.

[10] D. S. Brauer, Phosphate glasses, in Bio-glasses: an introduction, J. R. Jones and A. G. Clare, Eds., ed UK: John Wiley and Sons, Ltd., 2012, pp. 45-64.

[11] X. Liu, D. M. Grant, G. Palmer, A. J. Parsons, C. D. Rudd, and I. Ahmed, Magnesium coated phosphate glass fibers for unidirectional reinforcement of polycaprolactone composites, J Biomed Mater Res B Appl Biomater, vol. 103, pp. 1424-32, Oct 2015.

[12] I. Ahmed, M. Lewis, I. Olsen, and J. C. Knowles, Phosphate glasses for tissue engineering: Part 2. Processing and characterisation of a ternary-based P2O5–CaO–Na2O glass fibre system, Biomaterials, vol. 25, pp. 501-507, 2004.

[13] N. Sharmin, M. S. Hasan, A. J. Parsons, D. Furniss, C. A. Scotchford, I. Ahmed, et al., Effect of boron addition on the thermal, degradation, and cytocompatibility properties of phosphate-based glasses, Biomed Res Int, vol. 2013, p. 902427, 2013.

[14] D. Carta, D. Qiu, P. Guerry, I. Ahmed, E. A. Abou Neel, J. C. Knowles, et al., The effect of composition on the structure of sodium borophosphate glasses, J Non Cryst Solids, vol. 354, pp. 3671-3677, 2008.

[15] D. Qiu, P. Guerry, I. Ahmed, D. M. Pickup, D. Carta, J. C. Knowles, et al., A high-energy X-ray diffraction, 31P and 11B solid-state NMR study of the structure of aged sodium borophosphate glasses, Mater Chem Phys, vol. 111, pp. 455-462, 2008.

[16] A. Saranti, I. Koutselas, and M. A. Karakassides, Bioactive glasses in the system CaO–B2O3–P2O5: Preparation, structural study and in vitro evaluation, J Non Cryst Solids, vol. 352, pp. 390-398, 2006.

[17] C. Tan, I. Ahmed, A. J. Parsons, N. Sharmin, C. Zhu, J. Liu, et al., Structural, thermal and dissolution properties of MgO- and CaO-containing borophosphate glasses: effect of Fe2O3 addition, J Mater Sci, vol. 52, pp. 7489-7502, 2017.

[18] M. Navarro, M.-P. Ginebra, J. Clément, M. Salvador, A. Gloria, and J. A. Planell, Physicochemical degradation of titania-stabilized soluble phosphate glasses for medical applications, J Am Ceram Soc, vol. 86, pp. 1345–1352, 2003.

[19] K. Dey, N. Sharmin, R. A. Khan, S. Nahar, A. J. Parsons, and C. D. Rudd, Effect of iron phosphate glass on the physico-mechanical properties of jute fabric-reinforced polypropylene-based composites, J Thermoplast Compos, vol. 24, pp. 695-711, 2011.

[20] S. Cozien-Cazuc, A. J. Parsons, G. S. Walker, I. A. Jones, and C. D. Rudd, Real-time dissolution of P40Na20Ca16Mg24 phosphate glass fibers, J Non Cryst Solids, vol. 355, pp. 2514-2521, 2009.

[21] R. A. Khan, A. J. Parsons, I. A. Jones, G. S. Walker, and C. D. Rudd, Degradation and interfacial properties of iron phosphate glass fiber-reinforced PCL-based composite for synthetic bone replacement materials, Polym-Plast Technol, vol. 49, pp. 1265-1274, 2010.

[22] P. Haque, I. Ahmed, A. Parsons, R. Felfel, G. Walker, and C. Rudd, Degradation properties and microstructural analysis of 40P2O5-24MgO-16CaO-16Na2O-4Fe2O3 phosphate glass fibres, J Non Cryst Solids, vol. 375, pp. 99-109, 2013.

[23] I. Ahmed, A. Parsons, A. Jones, G. Walker, C. Scotchford, and C. Rudd, Cytocompatibility and effect of increasing MgO content in a range of quaternary invert phosphate-based glasses, J Biomater Appl, vol. 24, pp. 555-75, Feb 2010.

[24] M. Navarro, M.-P. Ginebra, and J. A. Planell, Cellular response to calcium phosphate glasses with controlled solubility, J Biomed Mater Res A., vol. 67, pp. 1009-1015, 2003.
[25] M. Uo, M. Mizuno, Y. Kuboki, A. Makishima, and F. Watari, Properties and cytotoxicity of water soluble Na2O–CaO–P2O5 glasses, Biomaterials, vol. 19, pp. 2277–2284, 1998.
[26] V. Salih, K. Franks, M. James, G. W. Hastings, J. C. Knowles, and I. Olsen, Development of soluble glasses for biomedical use Part II: The biological response of human osteoblast cell lines to phosphate-based soluble glasses, J Mater Sci-Mater M, vol. 11, pp. 615-620, 2000.
[27] A. Hoppe, N. S. Guldal, and A. R. Boccaccini, A review of the biological response to ionic dissolution products from bioactive glasses and glass-ceramics, Biomaterials, vol. 32, pp. 2757-74, Apr 2011.
[28] D. S. Brauer, C. Russel, W. Li, and S. Habelitz, Effect of degradation rates of resorbable phosphate invert glasses on in vitro osteoblast proliferation, J Biomed Mater Res A, vol. 77, pp. 213-9, May 2006.
[29] C. Albon, D. Muresan, R. E. Vandenberghe, and S. Simon, Iron environment in calcium-soda-phosphate glasses and vitroceramics, J Non Cryst Solids, vol. 354, pp. 4603-4608, 2008.
[30] M. Elisa, R. Iordanescu, B. A. Sava, G. Aldica, V. Kuncser, C. Valsangiacom, et al., Optical and structural investigations on iron-containing phosphate glasses, J Mater Sci vol. 46, pp. 1563-1570, 2010.
[31] B. C. Sales and L. A. Boatner, Physical and chemical characteristics of lead-iron phosphate nuclear waste glasses, J Non Cryst Solids, vol. 79, pp. 83-116, 1986.
[32] X. Yu, D. E. Day, G. J. Long, and R. K. Brow, Properties and structure of sodium-iron phosphate glasses, J Non Cryst Solids, vol. 215, pp. 21-31, 1997.
[33] R. Stefan and M. Karabulut, Structural properties of iron containing calcium-magnesium borophosphate glasses, J Mol Struct, vol. 1071, pp. 45-51, 2014.
[34] N. Sharmin, C. D. Rudd, A. J. Parsons, and I. Ahmed, Structure, viscosity and fibre drawing properties of phosphate-based glasses: effect of boron and iron oxide addition, J Mater Sci, vol. 51, pp. 7523-7535, 2016.
[35] P. Bergo, S. T. Reis, W. M. Pontuschka, J. M. Prison, and C. C. Motta, Dielectric properties and structural features of barium-iron phosphate glasses, J Non Cryst Solids, vol. 336, pp. 159-164, 2004.
[36] D. A. Magdas, O. Cozar, V. Chis, I. Ardelean, and N. Vedeanu, The structural dual role of Fe2O3 in some lead-phosphate glasses, Vib Spectrosc, vol. 48, pp. 251-254, 2008.
[37] M. Lu, F. Wang, Q. Liao, K. Chen, J. Qin, and S. Pan, FTIR spectra and thermal properties of TiO2-doped iron phosphate glasses, J Mol Struct, vol. 1081, pp. 187-192, 2015.
[38] B. Raguenet, G. Tricot, G. Silly, M. Ribes, and A. Pradel, The mixed glass former effect in twin-roller quenched lithium borophosphate glasses, Solid State Ionics, vol. 208, pp. 25-30, 2012.
[39] U. Hoppe, M. Karabulut, E. Metwalli, R. K. Brow, and P. J'ov'ari, The Fe-O coordination in iron phosphate glasses by XRD with high energy photons, Phys.: Condens. Matter, vol. 15, pp. 6143–6153, 2003.
[40] T. Okura, T. Miyachi, and H. Monma, Properties and vibrational spectra of magnesium phosphate glasses for nuclear waste immobilization, J Eur Ceram Soc, vol. 26, pp. 831-836, 2006.
[41] P. Y. Shih and T. S. Chin, Preparation of lead-free phosphate glasses with low Tg and excellent chemical durability, J Mater Sci Lett, vol. 20, pp. 1811 – 1813, 2001.
[42] D. N. Singh, Periodic Table and Periodicity of Properties in Basic Concept of Inorganic Chemistry D. N. Singh, Ed., ed India: Pearson Education 2009, pp. 1-32.
[43] R. M. Felfel, I. Ahmed, A. J. Parsons, P. Haque, G. S. Walker, and C. D. Rudd, Investigation of crystallinity, molecular weight change, and mechanical properties of PLA/PBG bioresorbable composites as bone fracture fixation plates, J Biomater Appl, vol. 26, pp. 765-789, Mar 2012.
[44] N. Han, I. Ahmed, A. J. Parsons, L. Harper, C. A. Scotchford, B. E. Scammell, et al., Influence of screw holes and gamma sterilization on properties of phosphate glass fiber-reinforced composite bone plates, J Biomater Appl, vol. 27, pp. 990-1002, May 2013.
[45] F. Barrera Betanzos, M. Gimeno-Fabra, J. Segal, D. Grant, and I. Ahmed, Cyclic pressure on compression-moulded bioresorbable phosphate glass fibre reinforced composites, Materials & Design, vol. 100, pp. 141-150, 2016.
[46] Q. Fu, E. Saiz, M. N. Rahaman, and A. P. Tomsia, Bioactive glass scaffolds for bone tissue engineering: state of the art and future perspectives, Mater Sci Eng C Mater Biol Appl, vol. 31, pp. 1245-1256, Oct 10 2011.
[47] R. M. Felfel, I. Ahmed, A. J. Parsons, L. T. Harper, and C. D. Rudd, Initial mechanical properties of phosphate-glass fibre-reinforced rods for use as resorbable intramedullary nails, Journal of Materials Science, vol. 47, pp. 4884-4894, 2012.
[48] M. R. Bosisio, M. Talmant, W. Skalli, P. Laugier, and D. Mitton, Apparent Young's modulus of human radius using inverse finite-element method, J Biomech, vol. 40, pp. 2022-8, 2007.
[49] I. Ahmed, A. J. Parsons, G. Palmer, J. C. Knowles, G. S. Walker, and C. D. Rudd, Weight loss, ion release and initial mechanical properties of a binary calcium phosphate glass fibre/PCL composite, Acta Biomater, vol. 4, pp. 1307-14, Sep 2008.
[50] P. Haque, A. J. Parsons, I. A. Barker, I. Ahmed, D. J. Irvine, G. S. Walker, et al., Interfacial properties of phosphate glass fibres/PLA composites: Effect of the end functionalities of oligomeric PLA coupling agents, Compos Sci Technol, vol. 70, pp. 1854-1860, 2010.
[51] N. Sharmin and C. D. Rudd, Structure, thermal properties, dissolution behaviour and biomedical applications of phosphate glasses and fibres: a review, J Mater Sci, vol. 52, pp. 8733-8760, 2017.
[52] R. K. Brow, Review: the structure of simple phosphate glasses, Journal of Non-Crystalline Solids, vol. 263&264, pp. 1-28, 2000.
[53] V. Pukh, L. Baikova, and T. Pesina, Structural strength of glass, in the Second Conference of the European Society of Glass Science and Technology, Stazione Sperimentale del Vetro, Venice, Italy, 1993, pp. 339-344.
[54] V. P. Pukh, L. G. Baikova, M. F. Kireenko, L. V. Tikhonova, T. P. Kazannikova, and A. B. Sinani, Atomic structure and strength of inorganic glasses, Physics of the Solid State, vol. 47, pp. 876–881, 2005.
[55] M. S. Hasan, Phosphate glass fibre reinforced composite for bone repair applications: Investigation of interfacial integrity improvements via chemical treatments, Doctor of Philosophy, The University of Nottingham, 2012.
[56] L. G. Baikova, Y. K. Fedorov, V. P. Pukh, T. I. Pesina, T. P. Kazannikova, L. V. Tikhonova, et al., Effect of cation field strength on

the mechanical properties of R2O–Al2O3–P2O5 glasses, Glass Phys Chem+, vol. 19, pp. 380–383, 1993.
[57] I. Ahmed, C. A. Collins, M. P. Lewis, I. Olsen, and J. C. Knowles, Processing, characterisation and biocompatibility of iron-phosphate glass fibres for tissue engineering, Biomaterials, vol. 25, pp. 3223-32, Jul 2004.
[58] M. S. Hasan, I. Ahmed, A. J. Parsons, G. S. Walker, and C. A. Scotchford, Material characterisation and cytocompatibility assessment of quinternary phosphate glasses, J Mater Sci-Mater M, vol. 23, pp. 2531-41, Oct 2012.
[59] L. Ma, R. K. Brow, and M. E. Schlesinger, Dissolution behavior of Na 2 O–FeO–Fe 2 O 3 –P 2 O 5 glasses, Journal of Non-Crystalline Solids, vol. 463, pp. 90-101, 2017.
[60] C. R. Kurkjian, Mechanical properties of phosphate glasses, J Non Cryst Solids, vol. 263-264, pp. 207–212, 2000.
[61] S. T. Lin, S. L. Krebs, S. Kadiyala, K. W. Leong, W. C. LaCourse, and B. Kumar, Development of bioabsorbable glass fibres, Biomaterials, vol. 15, pp. 1057-1061, 1994.
[62] J. B. Murgatroyd, The delayed elastic effect in glass fibres and the constitution of glass in fibre form, Journal of the Society of Glass Technology, vol. 32, pp. 291-300, 1948.
[63] R. J. Kirkpatrick and R. K. Brow, Nuclear magnetic resonance investigation of the structures of phosphate and phosphate-containing glasses: a review, Solid State Nucl Mag, vol. 5, pp. 9-21, 1995.
[64] W. Vogel and W. Höland, The development of bioglass ceramics for medical application, Angewandte Chemie International Edition, vol. 26, pp. 527-544, 1987.
[65] F. Döhler, A. Mandlule, L. v. Wüllen, M. Friedrich, and D. S. Brauer, 31P NMR characterisation of phosphate fragments during dissolution of calcium sodium phosphate glasses, J. Mater. Chem. B, vol. 3, pp. 1125-1134, 2015.
[66] B. C. Bunker, G. W. Arnold, and J. A. Wilder, Phosphate glass dissolution in aqueous solutions, J Non Cryst Solids, vol. 64, pp. 291-316, 1984/05/01/ 1984.
[67] H. Gao, T. Tan, and D. Wang, Dissolution mechanism and release kinetics of phosphate controlled release glasses in aqueous medium, J Control Release, vol. 96, pp. 29-36, Apr 16 2004.
[68] E. El-Meliegy, M. M. Farag, and J. C. Knowles, Dissolution and drug release profiles of phosphate glasses doped with high valency oxides, J Mater Sci Mater Med, vol. 27, p. 108, Jun 2016.
[69] S. E. Ruiz Hernandez, R. I. Ainsworth, and N. H. de Leeuw, Molecular dynamics simulations of bio-active phosphate-based glass surfaces, Journal of Non-Crystalline Solids, vol. 451, pp. 131-137, 2016.
[70] J. Clément, J. M. Manero, and J. A. Planell, Analysis of the structural changes of a phosphate glass during its dissolution in simulated body fluid, Materials Science: Materials Medicine vol. 10, pp. 729-732, 1999.
[71] I. Ahmed, J. J. Blaker, A. Bismarck, A. R. Boccaccini, M. P. Lewis, S. N. Nazhat, et al., Effect of iron on the surface, degradation and ion release properties of phosphate-based glass fibres, Acta Biomater, vol. 1, pp. 553-63, Sep 2005.
[72] S. Cozien-Cazuc, A. J. Parsons, G. S. Walker, I. A. Jones, and C. D. Rudd, Effects of aqueous aging on the mechanical properties of P40Na20Ca16Mg24 phosphate glass fibres, J Mater Sci, vol. 43, pp. 4834-4839, 2008.
[73] M. G. Mesko and D. E. Day, Immobilization of spent nuclear fuel in iron phosphate glass, J Nucl Mater, vol. 273, pp. 27-36, 1999.
[74] H. Stockhorst and R. Brückner, Structure sensitive measurements on phosphate glass fibers, J Non Cryst Solids, vol. 85, pp. 105-126, 1986.
[75] J. B. Murgatroyd, The strength of glass fibres, Part 1: elastic properties, Journal of the Society of Glass Technology, vol. 28, pp. 368-387, 1944.
[76] J. Choueka, J. L. Charvet, H. Alexander, Y. H. Oh, G. Joseph, N. C. Blumenthal, et al., Effect of annealing temperature on the degradation of reinforcing fibers for absorbable implants, Journal of Biomedical Materials Research, vol. 29, pp. 1309-1315, 1995.
[77] A. G. Metcalfe and G. K. Schmitz, Mechanisms of stress corrosion in E-glass filaments, Glass Technology, vol. 13, pp. 5-16, 1972.
[78] G. K. Schmitz and A. G. Metcalfe, Stress corrosion of E-glass fibers, Industrial & Engineering Chemistry Product Research and Development, vol. 5, pp. 1-8, 1966.
[79] S. Inaba, H. Hosono, and S. Ito, Entropic shrinkage of an oxide glass, Nature Materials, vol. 14, pp. 312–317, 2015.
[80] A. J. Parsons, I. Ahmed, J. Yang, S. Cozien-Cazuc, and C. D. Rudd, Heat-treatment of phosphate glass fibres and its effect on composite property retention presented at the 16th international conference on composite materials Kyoto, 2007.
[81] E. Pirhonen, H. Niiranen, T. Niemela, M. Brink, and P. Tormala, Manufacturing, mechanical characterization, and in vitro performance of bioactive glass 13-93 fibers, J Biomed Mater Res B Appl Biomater, vol. 77, pp. 227-33, May 2006.
[82] F. Muñoz, O. Pritula, J. Sedláček, and C. Rüssel, A study on the anisotropy of phosphate glass fibres, Glass Technol-Part A, vol. 49, pp. 47-52, 2008.